A&A 488, 323–329 (2008)
DOI: 10.1051/0004-6361:20079315

Astronomy & Astrophysics

Magnetic topology of blinkers⋆

S. Subramanian[1], M. S. Madjarska[2], R. C. Maclean[1,⋆⋆], J. G. Doyle[1], and D. Bewsher[3]

[1] Armagh Observatory, College Hill, Armagh BT61 9DG, N. Ireland
[2] Max-Planck-Institut für Sonnensystemforschung, Max-Planck-Str. 2, 37191 Katlenburg-Lindau, Germany
[3] Space Physics Division, Space Science and Technology Department, STFC Rutherford Appleton Laboratory, Chilton, Didcot, Oxfordshire, OX11 0QX, UK

Received 21 December 2007 / Accepted 17 June 2008

ABSTRACT

Context. Co-spatial and co-temporal spectroscopic, imaging and magnetogram data enable us to better understand various solar transient phenomena. Here, we study brightening events in the transition region of the quiet Sun, also called "blinkers".
Aims. We aim to investigate the physical mechanism responsible for blinkers.
Methods. An automated blinker identification procedure (BLIP) is used to identify blinker events in SoHO/CDS data. The 3D magnetic topology of the magnetic field in the blinker region is reconstructed based on SoHO/MDI magnetogram data.
Results. During 3 h of SoHO/CDS observations on 2006 January 18, 66 blinkers were identified in the O V 629 Å emission line. Out of them, a group comprising of 16 events were modelled here. They were found to be associated with the emergence of magnetic flux which gave rise to the appearance of, and multiple magnetic reconnection events across, an upper atmosphere (coronal) magnetic null point, along with a loop structure as observed with TRACE.
Conclusions. This blinker group results from the release of energy that was accumulated during flux emergence, although whether all blinkers follow the same formation scenario requires further investigation using additional multi-instrument/multi-mission studies.

Key words. Sun: activity – Sun: UV radiation – Sun: transition region – Sun: atmosphere – Sun: corona – Sun: magnetic fields

1. Introduction

Over the last decade, the field of solar physics has seen a tremendous improvement in its data acquisition capabilities. The increased use of space observatories such as the Solar and Heliospheric Observatory (SoHO) and the Transition Region and Coronal Explorer (TRACE), has brought many new features on the Sun to light. One of these new features, known as *blinkers*, represents Extreme-UltraViolet (EUV) brightenings, first reported by Harrison (1997) using the SoHO/Coronal Diagnostic Spectrometer (CDS; Harrison et al. 1995). They are most readily identified in the O V 629 Å transition region line ($T_{\max} \approx 2 \times 10^5$ K), but significant enhancements can also be seen in chromospheric lines like He I 584 Å ($T_{\max} \approx 5 \times 10^4$ K). Berghmans et al. (1998) identified many brightenings in EIT He II 304 Å having characteristics completely compatible with CDS blinkers, and suggested that they were reconnection events of low-lying quiet Sun (QS) loops.

Lightcurves of blinkers are separated into two distinct classes: simple blinkers with a smooth increase in intensity having only one significant peak; and complex blinkers with multiple significant peaks (Brković & Peter 2004). Table 1 shows the properties of blinkers derived from CDS and SUMER observations by Brković et al. (2001); Bewsher et al. (2002); Parnell et al. (2002); Madjarska & Doyle (2003); Bewsher et al. (2003); Tomasz et al. (2003).

Blinkers are located above regions of enhanced emission, such as network boundaries in the quiet Sun (Bewsher et al. 2002). Most blinkers were also found to be preferentially located near regions of prominent unipolar magnetic field in both the QS and active regions (Bewsher et al. 2002; Parnell et al. 2002). Doyle et al. (2004) showed an example of a blinker that was caused by the emergence of new magnetic flux.

Chae et al. (2000), Madjarska & Doyle (2003) and Bewsher et al. (2005) identified blinkers in SUMER and CDS simultaneous observations. They found that CDS blinkers consist of many small-scale, short-lived SUMER brightenings lasting 2–3 min and having a typical size of 3″–5″. Chae et al. (2000) suggested that these brightenings are produced by small-scale reconnections of network threads.

A number of theoretical models have been suggested to explain the mechanism responsible for creating blinkers. Harrison et al. (1999) proposed a model which consists of merging of closed loops. Tarbell et al. (1999) put forward a model where reconnection of intense magnetic flux tubes of opposite polarity, in a photospheric environment that is otherwise free of magnetic field, results in a sling-shot effect generating pure acoustic waves. These waves can steepen and create shocks. Depending on the geometry of the collision of the flux tubes, the energy may be converted into either heat or jets, or indeed both.

According to Priest et al. (2002), blinkers may be formed by one of five different mechanisms: (i) the heating of cool spicular material; (ii) the containment of the plasma in the low lying loops in the network; (iii) thermal linking of hot and cold plasma at the feet of coronal loops; (iv) heating and evaporation of chromospheric plasma driven by granular compression; and (v) the cooling and draining of hot coronal plasma when coronal heating is switched off.

Peter & Brković (2003) studied blinkers with SUMER and showed that their decreasing line-width corresponded to an

⋆ 2 movies are only available in electronic form at http://star.arm.ac.uk/preprints/ and http://www.aanda.org

⋆⋆ *Now at*: School of Mathematics and Statistics, University of St Andrews, North Haugh, St Andrews, Fife, KY16 9SS, UK.

Table 1. Main properties of CDS blinkers.

Blinker property	Quiet sun value	Active region value
Mean lifetime (minutes)	16[1], 16[2]	17.5[3]
Mean area ($\times 10^7$ km^2)	2.4[1], 3.0[2]	4.0[3]
Mean enhancement factor	1.8[2]	2.4[3]
Global frequency (s^{-1})	22[1], 7.5[2]	13.7[3]
Doppler velocities (km s^{-1})	5–25 (N V)[4], 15 (O VI)[5], 10–15 (He I)[6], 25–30 (O V)[6]	10–20 (He I)[6], 20–40 (O V)[6]
Non-thermal velocities (km s^{-1})	15–25(He I)[6], 30–45 (O V)[6]	15–25(He I)[6], 30–45 (O V)[6]

[1] Brković et al. (2001); [2] Bewsher et al. (2002); [3] Parnell et al. (2002); [4] Madjarska & Doyle (2003); [5] Tomasz et al. (2003); [6] Bewsher et al. (2003).

increase in the Doppler shift, suggesting that they are driven by events in the chromosphere which heat a loop asymmetrically and power a strong laminar flow through the loops. Doyle et al. (2004) suggested that blinkers may be associated with brightenings in pre-existing coronal loops, which are triggered during the reconnection between the newly emerging magnetic flux and the pre-existing flux.

Based on the above, it is clear that there is still an ongoing debate on the physical mechanism responsible for blinkers. This motivated us to conduct a multi-instrument observing campaign including spectral, imaging, and magnetic field measurements of the QS. Topological analysis of the magnetic field in the blinker region is central to this study, as we wish to investigate whether blinkers are powered by magnetic reconnection or its effects. In Sect. 2 we discuss the observational data used, including their reduction and the co-alignment procedure. In Sect. 3, we discuss the blinker identification and the overall appearance of the blinkers in the different images, then we outline the results obtained via the magnetic topology analysis.

2. Observations and data reduction

Simultaneous observations with SoHO/CDS, SoHO/EIT (Extreme-Ultraviolet Imaging Telescope; Delaboudinière et al. 1995), SoHO/MDI (Michelson Doppler Imager; Scherrer et al. 1995) and TRACE (Transition Region and Coronal Explorer; Handy et al. 1999) were obtained near disk centre on 2006 January 18.

CDS was observing in a rastering mode in He I 584 Å, He II 304 Å (seen in second order), O V 629 Å and a spectral window centred around 560 Å containing Ca X and Ne VI lines. The data consist of a large raster with a field-of-view (FOV) of 240″ × 240″ followed by 40 small rasters with a FOV of 40″ × 124″ taken with a cadence of 4 min and a pixel size of 4″ × 1.68″. The data were reduced using the standard software packages for the correction of missing pixels, cosmic ray hits, CCD bias effects and flat-field effects. The non-standard tilt correction of Bewsher et al. (2003) was also applied. An intensity map of the emission from each spectral window was obtained by integrating over the spectral line.

The EIT He II images were taken in a shutterless mode and have a FOV of 1090″ × 1090″, with a cadence of 1 min and a pixel size of 2.63″ × 2.63″ (for details on EIT shutterless observations and data reduction see Madjarska et al. 2006).

TRACE images were obtained in the 1550 Å channel with a FOV of 384″ × 384″, a cadence of 15 s and a pixel size of 0.5″ × 0.5″.

High-resolution photospheric line-of-sight magnetograms were obtained with MDI at a cadence of 1 min with a pixel size of 0.6″ × 0.6″. They were preprocessed by taking a running average over five minutes, to reduce high-frequency noise and filter out the ubiquitous five-minute oscillations.

The images from the different instruments were co-aligned in order to follow the same FOV for further analysis. First, the EIT He II images were aligned with respect to the TRACE 1550 Å images as they share large fields-of-view. Next, the MDI magnetograms were aligned with the TRACE 1550 Å images using the continuum contribution for comparison. Finally, the CDS He II 304 Å (2nd order) raster images were aligned with the EIT He II 304 Å images.

An automated method of identifying blinkers (Blinker Identification Procedure or BLIP), developed by Bewsher et al. (2002), was used to identify blinkers in the CDS O V 629 Å rasters. The procedure identifies group of n_p pixels that have significant temporal peaks, where n_p is an integer which is user specified. It identifies peaks in the data that have an intensity increase which is larger than $n_\lambda \times \lambda$, where λ is the value below which 99% of the Poisson errors occur and n_λ is a user-specified integer. For this paper, we used $n_p = 2$ and $n_\lambda = 5$. Varying these parameters changes the number of events identified, but does not significantly change the average properties of the events identified. See Table 1 in Bewsher et al. (2002) for further details.

The preprocessed photospheric MDI magnetograms were used as boundary conditions to reconstruct the three-dimensional (3D) structure of the magnetic field in the atmosphere above. We identified many distinct magnetic features (isolated regions of strong positive or negative line-of-sight magnetic field) on each magnetogram. Here we chose to explicitly define a magnetic feature as a group of at least four contiguous pixels with at least one pixel having an unsigned magnetic flux above 20 G and the rest having magnetic fluxes greater than 10 G. This choice of threshold values is a good compromise (at least for this dataset), allowing the reliable detection of faint magnetic features without also including a high level of noise.

The evolution of the magnetic features was tracked between frames using the YAFTA feature-tracking software (Welsch et al. 2004; DeForest et al. 2007). All the features thus identified were then further reduced to magnetic point sources, with the strength of each point source proportional to the total integrated magnetic flux in the parent feature, and the location of each point source given by the flux-weighted centre of the parent feature. For example, the x-coordinate of a point source derived from a parent feature consisting of N_i pixels, where pixel i is located at x_i with magnetic field strength B_i, is given by:

$$x = \frac{\sum_{i=1}^{N_i} x_i B_i}{\sum_{i=1}^{N_i} B_i}. \quad (1)$$

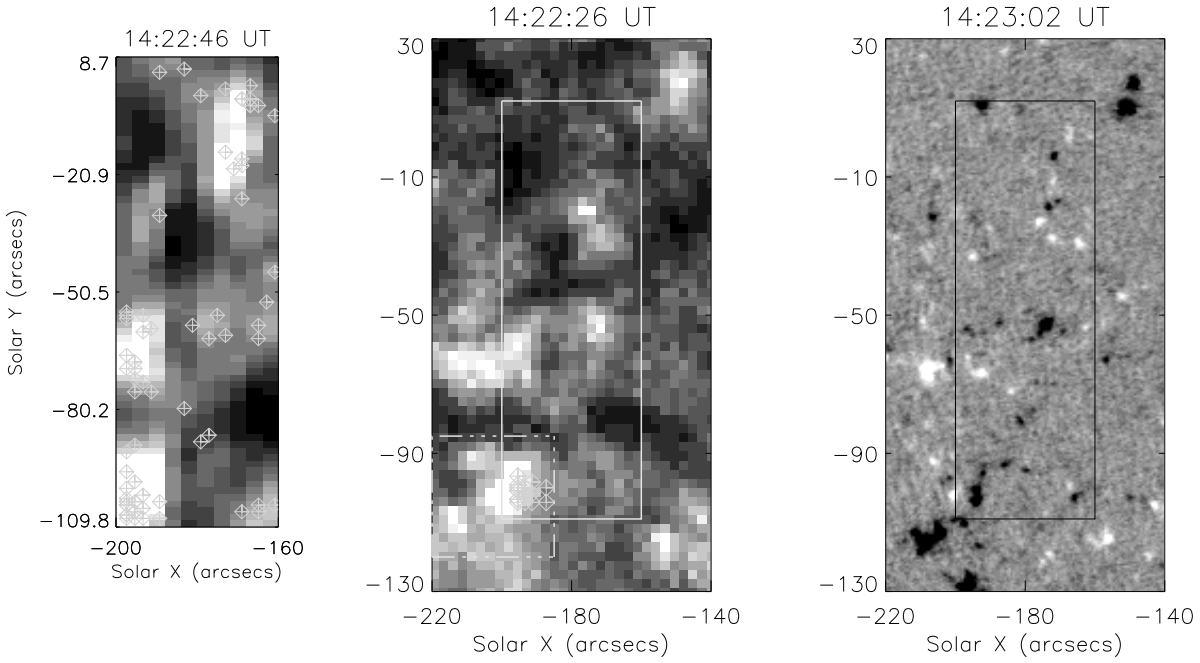

Fig. 1. CDS O v 629 Å raster (*left*). The diamonds mark the positions of blinkers identified with BLIP. EIT image in the He II 304 Å passband (*middle*). The solid line box shows the field-of-view of the CDS raster, the dot-dot-dot-dash box shows the field-of-view of the TRACE 1550 Å images presented further in this paper. The blinkers shown with diamonds in the lower left-hand corner of the CDS and TRACE 1550 Å fields-of-view were further analysed and modelled. MDI magnetogram (*right*) with a black solid box marking the position of the CDS FOV.

Similarly, the y-coordinate of the source can be computed by substituting y for x in Eq. (1).

For each frame, a simple potential magnetic field extrapolation was performed to model the 3D magnetic field, based on the set of point sources representing the magnetic features. A potential magnetic field was chosen for simplicity. This type of field is normally an acceptable first approximation to the true magnetic field in quiet Sun regions (Brown & Priest 2000) such as the region studied here. This is because, in the quiet Sun, the magnetic energy of the field is typically not much larger than that of the equivalent potential field, and so the topological structure of the potential field is a good guideline to the topological structure of the real coronal field, even if the detailed geometry is not identical.

2.1. Magnetic topology analysis

Finally, in order to study the structure and evolution of the magnetic field associated with the detected blinkers, the *magnetic charge topology* (MCT; Longcope 2005) of the resulting 3D magnetic field was analysed using the MPOLE topology software package (Longcope & Klapper 2002). Such an analysis involves locating the *magnetic null points* (Parnell et al. 1996) of the field, which are then used to find other topological features (Beveridge & Longcope 2005), such as *spine* fieldlines, *separatrix surfaces*, and *separators*. These features do not only provide a useful way to visualise the 3D magnetic connectivity of the field; they have also been shown to be associated with magnetic reconnection and coronal heating (McLaughlin & Hood 2006; Priest et al. 2005). In the next section, we look in some detail at the sequence of magnetic topological states derived for the blinker group region, and put forward our interpretation of its significance for the nature of the blinker phenomenon.

3. Results

Figure 1 (left) shows one of the 40 CDS rasters in the O v 629 Å line used for the blinker identification. An EIT He II 304 Å image with a larger FOV together with a corresponding MDI magnetogram gives a better overview of the observed region. We also created a movie which shows how the blinkers evolved over the course of the observations (see movie 1[1]).

We detected 66 blinkers in the CDS O v 629 Å line raster images, using the parameters described in Sect. 2. It is apparent that the blinkers are not uniformly distributed over the field-of-view; on the contrary, it appears that a number of blinkers occur close to each other. These show similar light curves and are associated with high concentrations of magnetic flux. We focused our further analysis on such a cluster of 16 blinkers occurring in the lower left-hand corner of the CDS rasters. The light curves of these individual events are very similar, suggesting a common emission mechanism. Figure 2 shows the lightcurve of this cluster as a whole over a region of 8″ × 12″, with a sample of 3 individual blinkers as seen in CDS O v 629 Å. For comparison, we also show the EIT He II 304 Å lightcurve.

In order to get more information about the studied blinkers we analysed a larger FOV of high-resolution TRACE images (with a spatial resolution six times better than EIT) and their corresponding magnetograms. In the TRACE 1550 Å images, a number of small-scale brightenings are continually appearing and fading across the entire region over the course of the observations. However, at the time the blinker group is seen in the CDS data, we observe the appearance of a loop structure in the TRACE images. The loop is partially outside the CDS FOV. The loop formation is associated with the emergence of

[1] See movie at http://star.arm.ac.uk/preprints/

new magnetic flux near the pre-existing magnetic flux of opposite polarity (Fig. 3) . The newly emerging positive polarity falls outside the CDS FOV. Note that the TRACE 1550 Å channel, despite having a wide passband of 30 Å, is strongly dominated by C IV 1548 Å and 1550 Å during transition region phenomena, such as blinkers (de Wijn et al. 2007).

Modelling of the magnetic topology of the blinker group shows that it goes through several major topological phases. Figure 3 shows three rows of images corresponding to the time before the appearance of the blinker group (top row), during the creation of the blinker group (middle row) and at the time of the blinker group activity (bottom row; see the lightcurve in Fig. 2 for comparison).

The central panel presents the photospheric footprints of the calculated magnetic topologies for the MDI frames in the left panel, while the right panel shows the formation of the loop structure resulting from the emergence of new magnetic flux as seen in the corresponding TRACE 1550 Å images.

The magnetic topology shortly before the blinkers (Fig. 3, top left) shows a large region of negative polarity towards the bottom edge of the image, consisting of several negative magnetic sources (including N1 and N2). It is one of the strongest source regions in the whole modelled area. There is also a weaker negative region towards the right-hand edge of the image, containing negative sources N3, N4, and N5, and a weak positive region P1. All of P1's magnetic flux connects to the negative sources just mentioned which are contained within the separatrix of the photospheric null which lies just to the north of P1.

Figure 4a shows a 3D plot of the separatrix dome of the null just north of P1. This dome contains all the magnetic flux from P1, and illustrates the structure of the background state, inside which the blinker group occurs a short time later. It is a simple structure topologically speaking, with no upper atmosphere (coronal) nulls and only one significant separator.

At 13:58 UT, P2 appears (see the middle row in Fig. 3). It represents the newly emerging positive flux at about (–203″, –103″) in solar disk coordinates. By 14:13 UT, P2 is strongly magnetically connected to N2 – not just to N3/N4 (which appear to be its partners in the flux emergence). This implies that significant magnetic reconnection had already taken place by this time to link P2 to N2. Its large-scale structure consists of two intersecting states, one separatrix dome clearly enclosed inside the other. The emergence of P2 (Fig. 4b) has complicated the topology, which now contains two significant separators; one from each positive null to the main negative null.

P2 gets stronger quickly and starts moving North-East, away from where it first appeared, and away from N3 and N4. At 14:16 UT, N7 appears and the topology changes again, to the state shown in the bottom row of Fig. 3.

The magnetic topology described above is a many-source version of an intersecting state as discussed by Beveridge et al. (2002). A classic intersecting state is a four-source state, as sketched in Fig. 5a; a separatrix "wall" from the negative null intersects a separatrix "dome" from the positive null (the intersection gives rise to a separator), and all of the magnetic flux from the positive source is divided between the two negative sources.

The real topology in Fig. 3 has P1 as the positive source, the group N1 and N2 as one negative source, and the group N3, N4, and N5 as the other negative source. The nulls between sources within each group are spurious, i.e. artifacts of the point source approximation, and may be disregarded, along with their associated spines and separatrices. The new topology is sketched in

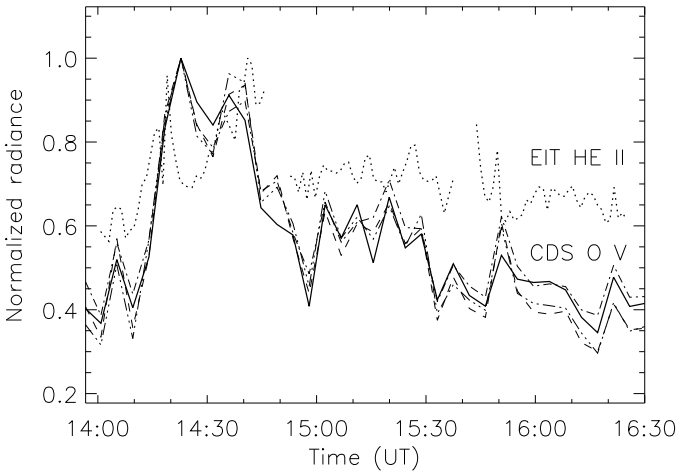

Fig. 2. Light curve of the blinker group (solid line), with the light curves for a sample of 3 individual blinkers (dashed and dotted line) as seen in CDS O V 629 Å. The EIT He II 304 Å light curve is shown for comparison.

Fig. 5b, while the main features of this final topological state are sketched in Fig. 5c. A positive upper atmosphere (coronal) null point appears in the topology at this time, and persists for over an hour, until about 15:24 UT. By upper atmosphere (coronal) null, we mean a null which does not lie on the boundary layer. The null may be located in the chromosphere, transition region or corona.

The null forms as a result of a topological bifurcation caused by the emergence of N7. It rises up along the pre-existing separator on the internal separatrix dome, so that the dome now belongs to the upper atmosphere (coronal) null. This topology is classified as a coronal null state enclosed within an intersecting state. The coronal null can be seen in Fig. 4c. It rises quickly and spends most of its lifetime sitting at about 1.5″ above the photospheric surface. Many separators are now present in what has become a complex topology. In particular, the creation of separators between the coronal null and the negative magnetic polarity region encompassing N3 and N4 may be linked to the birth of the blinker group.

Null points such as this newly-created one in the upper atmosphere are much rarer than the photospheric nulls that we have seen up to this point (Longcope et al. 2003). They are associated with magnetic reconnection and coronal heating (Fletcher et al. 2001), both because they connect to separatrix surfaces which themselves are prime locations for magnetic reconnection (Priest et al. 2005) and because coronal nulls can act as a focus for passing magnetoacoustic waves which then dump their energy at or near the null (McLaughlin & Hood 2006). The presence of the coronal null may facilitate magnetic reconnection by creating a new direct path for reconnection between two previously separate flux domains (Beveridge 2007, private communication).

In the present data, the upper atmosphere null appears in the topology at 14:16 UT, while the CDS light curve of the blinker group peaks at 14:20 UT (see Fig. 2), which strongly suggests that reconnection events at the new coronal null are associated with the brightening in the 16 blinkers.

To find out where this reconnection takes place, we investigated the magnetic connections from P2 to the negative sources: in particular, to which negative sources does P2 connect, at what times, and how strong are these connections? To find out, we randomly initiated 1000 fieldlines from P2 in each frame, and

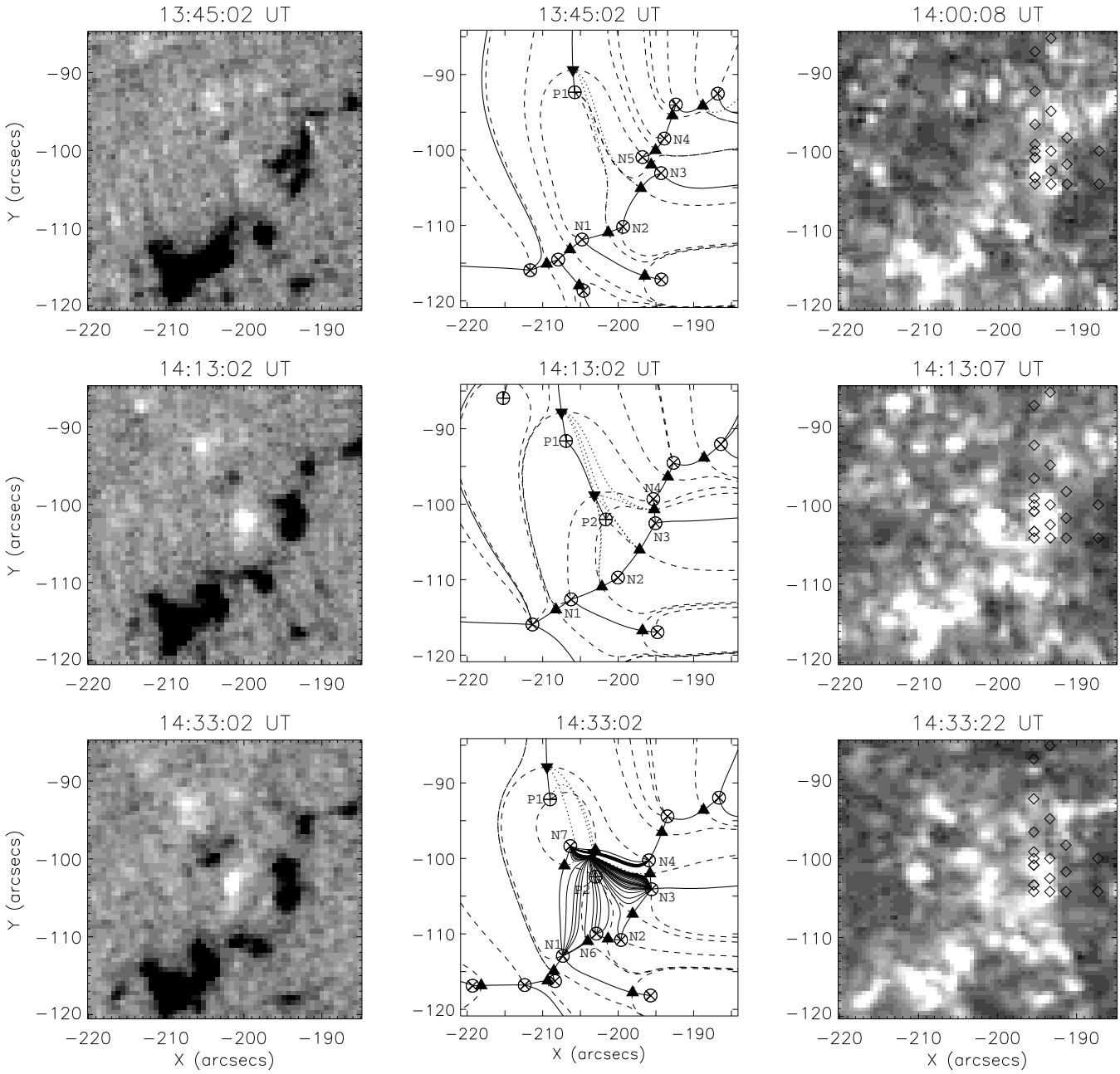

Fig. 3. *Left panel*: MDI snapshots (averaged over five minutes) illustrating the photospheric magnetic field during each of the three main topological phases of the blinker group. *Middle panel*: photospheric footprints of the magnetic topologies corresponding to the MDI images. Positive/negative magnetic point sources are labelled P/N and marked with ⊕/⊗ symbols. Positive/negative magnetic null points are marked with ▼/▲ symbols. Spines are shown as solid fieldlines, and dashed fieldlines indicate where separatrix surfaces intersect the photosphere. Separators (in the corona) are shown as dotted lines. In the final image (corresponding to 14:33 UT), fieldlines in the separatrix surface of the newly formed coronal null are shown as thin solid curves. *Right panel*: corresponding TRACE 1550 Å at 14:00 UT, 14:13 UT and 14:33 UT, note that the first available TRACE image is 15 min later than the MDI image.

recorded at which negative sources they terminated. Figure 6 shows the results.

The total magnetic flux of P2 decreases sharply at about 14:20 UT, corresponding with the time of the peak in the O v 629 Å lightcurve. At this time there is also a significant decrease in the magnetic flux connecting P2 to N1 and N2. Some of the flux disappears from the blinker group system altogether, and some goes into the new domain P2–N6. There are, therefore, several different reconnection events happening simultaneously. Flux is being transferred from one domain to another within the coronal null's separatrix surface, and it is also being transferred across the separatrix. The location of the observed brightening is determined by a complicated interplay between the location of the reconnecting flux domains, the length of the fieldlines in each domain, and the density of the plasma along the loops. We hope to extend our study to other similar regions in the near future in order to make some progress on understanding how the location of the blinkers are determined.

4. Discussion and conclusions

Here we present results from simultaneous spectral, imaging and magnetogram observations of a blinker group. We have found

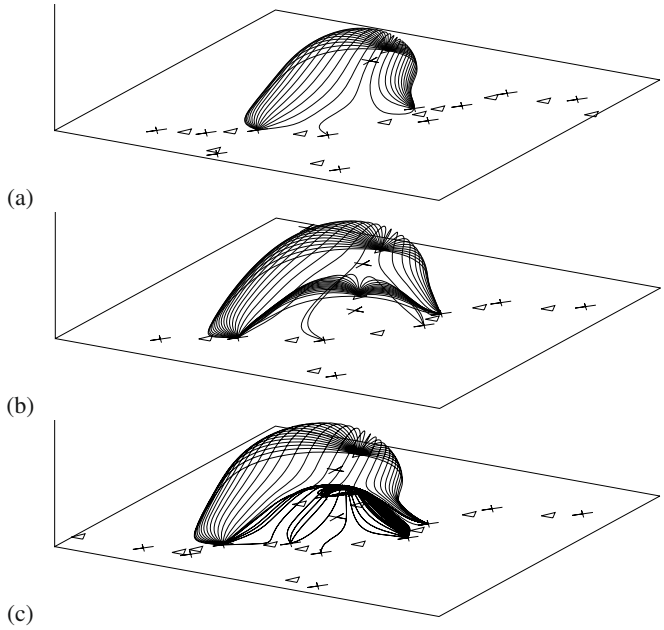

Fig. 4. Three-dimensional fieldline extrapolations showing the important topological separatrix surfaces for each of the three phases of the blinker group. **a)** The overlying separatrix dome which contains all the flux from P1 and bounds the entire blinker group region. **b)** The appearance of P2 creates a new separatrix dome inside the pre-existing one. **c)** The internal dome plays host to a new coronal null point.

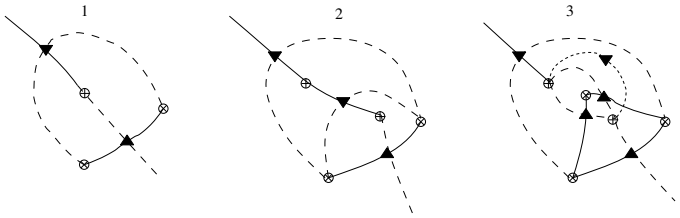

Fig. 5. A sequence of sketches of the important features in the topological footprints of the blinker group region during each of the three main phases. **a)** Is the initial intersecting state, **b)** is the second stage which consists of two intersecting states, one inside the other, and **c)** shows the final topology which includes a coronal null along with its associated spine. Positive sources are shown as ⊕, negative sources as ⊗, positive nulls as ▼, and negative nulls as ▲. Spines (in the photosphere) are solid curves, separatrix traces are dashed, and the spine of the coronal null is dotted.

that this blinker group is associated with loops forming after magnetic flux emergence.

A topological analysis of the 3D magnetic field of the blinker group shows that it progressed through three main topological phases. In the beginning there was a simple separatrix dome. As the topological complexity of the region increased and new magnetic source regions emerged, a second dome formed inside the first, and a coronal null appeared on the new dome. Flux emergence and reconnection across the coronal null and its associated separators, with the release of accumulated energy (as seen with TRACE and EIT), are likely to be the cause of the blinkers. Further work is needed to find out whether all blinkers follow the same formation scenario.

The magnetic topological model that we have used here to analyse the 3D magnetic field structure in the blinker group region has previously been used to model larger regions of the solar atmosphere. However it is equally valid on smaller length scales (such as the scale of the blinkers modelled here) so long as

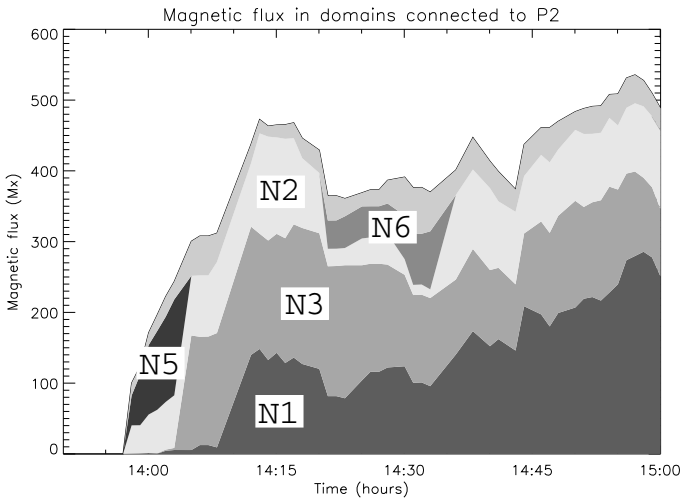

Fig. 6. The black line shows how the total magnetic flux available from P2 varies in time. Each shaded area represents the strength of the specific magnetic connection between P2 and a different named negative source. The unlabelled area at the *top* represents the contributions from all of P2's other magnetic connections, which are too weak to show individually.

the photospheric magnetogram data is of sufficiently high resolution to identify the main magnetic features involved. Any small unidentified magnetic sources that exist below a strength of 10 G may locally perturb the position of a topological feature by a very small distance, but will be too weak to affect the overall topological structure of the present blinker group region.

Such a magnetostatic model does not include temperature effects and therefore we cannot say whether the null above the photospheric plane is in the chromosphere, transition region, or corona. However, the radiative loss function of the plasma in the solar atmosphere has its maximum efficiency in the transition region, so we should expect to best see blinkers at transition region temperatures, particularly as they are not energetic enough to be observed in coronal lines. The topological model showed the null to be located about 1 Mm above the photosphere, an altitude which would place it in the transition region or lower corona. Several separators (also good locations for magnetic reconnection) join the atmospheric null to its photospheric counterparts, so reconnection along these separators, releasing enough energy to heat the plasma to transition region temperatures, could also contribute to powering the blinker.

Acknowledgements. We would like to thank the SoHO CDS & EIT teams plus the TRACE teams for their help in planning these observations. SoHO is a mission of international cooperation between ESA and NASA. Research at Armagh Observatory is grant-aided by the N. Ireland Department of Culture, Arts and Leisure. This work was supported in part by a PRTLI research grant for Grid-enabled Computational Physics of Natural Phenomena. R.C.M. is grateful for financial support from the UK Science and Technology Facilities Council.

References

Berghmans, D., Clette, F., & Moses, D. 1998, A&A, 336, 1039
Beveridge, C., & Longcope, D. W. 2005, Sol. Phys., 227, 193
Beveridge, C., Priest, E. R., & Brown, D. S. 2002, Sol. Phys., 209, 333
Bewsher, D., Parnell, C. E., & Harrison, R. A. 2002, Sol. Phys., 206, 21
Bewsher, D., Parnell, C. E., Pike, C. D., & Harrison, R. A. 2003, Sol. Phys., 215, 217
Bewsher, D., Innes, D. E., Parnell, C. E., & Brown, D. S. 2005, A&A, 432, 307
Brković, A., & Peter, H. 2004, A&A, 422, 709
Brković, A., Solanki, S. K., & Rüedi, I. 2001, A&A, 373, 1056
Brown, D. S., & Priest, E. R. 2000, Sol. Phys., 194, 197

Chae, J., Wang, H., Goode, P. R., Fludra, A., & Schühle, U. 2000, ApJ, 528, L119
de Wijn, A. G., De Pontieu, B., & Rutten, R. J. 2007, ApJ, 654, 1128
DeForest, C. E., Hagenaar, H. J., Lamb, D. A., Parnell, C. E., & Welsch, B. T. 2007, ApJ, 666, 576
Delaboudinière, J.-P., Artzner, G. E., Brunaud, J., et al. 1995, Sol. Phys., 162, 291
Doyle, J. G., Roussev, I. I., & Madjarska, M. S. 2004, A&A, 418, L9
Fletcher, L., Metcalf, T. R., Alexander, D., Brown, D. S., & Ryder, L. A. 2001, ApJ., 554, 451
Handy, B. N., Acton, L. W., Kankelborg, C. C., et al. 1999, Sol. Phys., 187, 229
Harrison, R. A. 1997, Sol. Phys., 175, 467
Harrison, R. A., Sawyer, E. C., Carter, M. K., et al. 1995, Sol. Phys., 162, 233
Harrison, R. A., Lang, J., Brooks, D. H., & Innes, D. E. 1999, A&A, 351, 1115
Longcope, D. W. 2005, Living Rev. Sol. Phys., 2, 7
Longcope, D. W., & Klapper, I. 2002, ApJ, 579, 468
Longcope, D. W., Brown, D. S., & Priest, E. R. 2003, Phys. Plasmas, 10, 3321
Madjarska, M. S., & Doyle, J. G. 2003, A&A, 403, 731
Madjarska, M. S., Doyle, J. G., Hochedez, J.-F., & Theissen, A. 2006, A&A, 452, L11
McLaughlin, J. A., & Hood, A. W. 2006, A&A, 459, 641
Parnell, C. E., Smith, J. M., Neukirch, T., & Priest, E. R. 1996, Physics of Plasmas, 3, 759
Parnell, C. E., Bewsher, D., & Harrison, R. A. 2002, Sol. Phys., 206, 249
Peter, H., & Brković, A. 2003, A&A, 403, 287
Priest, E. R., Hood, A. W., & Bewsher, D. 2002, Sol. Phys., 205, 249
Priest, E. R., Longcope, D. W., & Heyvaerts, J. 2005, ApJ, 624, 1057
Scherrer, P. H., Bogart, R. S., Bush, R. I., et al. 1995, Sol. Phys., 162, 129
Tarbell, T., Ryutova, M., Covington, J., & Fludra, A. 1999, ApJ, 514, L47
Tomasz, F., Rybák, J., Kučera, A., Curdt, W., & Wöhl, H. 2003, Hvar Obs. Bull., 27, 75
Welsch, B. T., Fisher, G. H., Abbett, W. P., & Regnier, S. 2004, ApJ, 610, 1148